NUMERICAL SIMULATION OF VORTICAL FLOW OVER A DELTA WING AT SUBSONIC AND TRANSONIC SPEEDS*)

H.W.M. Hoeijmakers, J.M.J.W. Jacobs and J.I. van den Berg
National Aerospace Laboratory NLR
Amsterdam, The Netherlands

Abstract

The flow about a 65-deg sharp-edged cropped delta wing is simulated by solving the Euler equations. Solutions are obtained for the wing of a subsonic, free-stream Mach number and high angle of attack, where a strong vortex forms above the wing upper surface as well as for the wing at a transonic free-stream Mach number and high incidence resulting in shocks and strong vortices. For the latter case the development of the flow field with the incidence is studied, while for both cases the formation of the wake downstream of the trailing edge is investigated. The influence of the mesh resolution on the details of the solution is analyzed utilizing a mesh of O-O topology with on its finest level more than one million grid points in the half-space around the starboard side of the delta wing.

Introduction

Vortex flow associated with flow separation from swept leading edges is of extreme importance for the high-angle-of-attack aerodynamics of fighter aircraft. For aerodynamically sharp leading edges the formation of the leading-edge vortex due to flow separation at the sharp edge (see Fig. 1) and the effect of the vortex on the flow over the upper surface of the wing is only slightly dependent on Reynolds number. This implies that this type of high-Reynolds-number flow can be simulated by inviscid flow models.

For the sub-critical flow about delta-like wings potential-flow methods have met some success in modelling leading-edge vortex flow (Ref. 1). In these methods the free shear layers are modelled by vortex sheets "fitted" into the potential flow field, i.e. one has to decide a priori on the presence of vortex sheets and vortex cores, although their position and strength is determined as part of the solution. This implies, that the topology of the flow must be well-defined and known in advance.

A mathematical model based on the Euler equations allows for rotational flow everywhere in the flow field and numerical methods based on it are able to capture, along with shock waves, vortical flow regions as an integral part of the discrete solution. This renders computational methods based on Euler's equations rather attractive for cases with a complex vortex flow pattern. This is particularly true for transonic flow with vortices and with (strong) shock waves, where there is the additional complexity of the mutual interaction of these two non-lineair flow phenomena. The computer resources required for an Euler method can be met by present-day supercomputers and Euler methods begin to demonstrate their capabilities for attached flows, including cases with propeller-slipstream interactions, and in particular for the high-angle-of-attack separated flows such as leading-edge vortex flow.

In the literature many computational investigations report on predicting the steady vortex-dominated flow based on the Euler equations (Refs. 2-7), addressing various aspects of the numerical simulation of this type of flow.

Viscous effects neglected in an Euler method, which are known to be responsible for the occurrence of secondary separation (see Fig. 1) and which affect the development of the flow near the center of the primary vortex core, will have to be assessed through a more elaborate model of the flow. Several investigations have already made efforts utilizing a Navier-Stokes method (Refs. 8-10) to simulate the flow about wings with leading-edge vortex separation. Navier-Stokes methods, however, require compared to Euler methods fine grids to resolve the relative small-scale viscous effects, leading to large computer time requirements.

One of the motivations of the present investigation using an Euler method was to study the effects of grid refinement on the solution and especially on the artificial dissipation. The latter is introduced explicitly by the numerical algorithm and implicitly by the non-uniformity of the grid, the implementation of the far-field boundary conditions, the treatment of the solid-wall boundary condition (see Ref. 11), etc.
The influence of the mesh resolution on the details of the Euler solution will be analyzed utilizing a grid with more than one million cells on its finest level.

In the present paper the Euler method under development at NLR is applied to the simulation of the flow about a 65-deg sharp-edged cropped delta wing at subsonic and transonic speed. The wing has a taper ratio of 0.15. The chordwise airfoil section is the NACA 64A005 airfoil which upstream of its point of maximum thickness (0.4 c) is smoothly blended into a biconvex shape. For this configuration, with an under-wing body, experimental data is available (Refs. 12, 13) and the flow structure is reasonably well known. It is presumed that the presence of the body has only a small effect on the flow field away from the apex of the wing. Earlier computational results on different aspects of the simulation have been reported in Ref. 14.

Outline of the methods used

The computational mesh is obtained using the grid generator developed at NLR (Ref. 14). This grid generator produces multi-blocked surface-fitted grids initialized through transfinite interpolation and tuned through a method based on a system of elliptic partial differential equations. The

*) This investigation has been carried out under contract with the Netherlands Agency for Aerospace Programs (NIVR) for the Netherlands Ministry of Defence.

grid lines are continuous but may be slope-discontinuous across block boundaries.
The Euler method (Ref. 16) used solves the time-dependent Euler equations employing the fully-conservative, cell-centered scheme of Jameson et al. (Ref. 17). The five equations in integral form for the conservation of mass, momentum and energy are discretized using a central-difference scheme. Fourth-difference dissipative terms are added to the discretized equations to provide the background dissipation that suppresses the tendency for odd-even point solution decompling. In regions with large pressure gradients, e.g. near shock waves and stagnation points, second-difference dissipative terms take over to damp pre- and post-shock oscillations.
To obtain a steady-state solution, integration in time is carried out by a four-stage Runge-Kutta scheme, in which the dissipative terms are evaluated at the first step only. Convergence to a steady state is accelerated by the application of local time-stepping, enthalpy damping and residual averaging.
For the conditions on the solid surface the method employs a linear extrapolation of the pressure from the flow field to the wall. The boundary conditions at the outer boundary of the computational domain are implemented using Riemann invariants.

The numerical flow simulation system at NLR can handle a grid with a multi-block structure, implementing a special boundary condition at internal blok interfaces to accommodate possibly slope-discontinuous grid lines and jumps in cell size across block boundaries. It is permitted to have a grid with degenerated cells, i.e. cells with faces and/or edges collapsed to a line or a point.

Grids

For the present investigations two (8-block) grids have been used to compute the flow about the cropped delta wing. A "fine" grid, 0-0 topology, has been generated around the starboard half of the wing. This grid has grid dimensions 288x76x56 (1,225,728 cells), that is in chordwise direction, 144 cells on both the wing upper and lower surface, in spanwise direction 76 cells and 56 cells between the wing surface and the outer boundary of the computational domain. It is symmetric with respect to the horizontal plane of symmetry of the wing. By combining groups of eight cells a "medium" grid with dimensions 144x38x28 (153,216 cells) has been extracted from the fine grid.
On the forward portion of the wing surface the grid is "conical" as can be seen in Fig. 2 which shows details of the medium grid. This quasi-conical arrangement of the grid preserves the grid resolution near the apex. Grid lines are clustered near the apex, near the leading edge and near the trailing edge. Near the wing, i.e. in the region where large gradients in the flow quantities are expected, the cell stretching ratio has been kept close to unity.
The outer boundary of the computational domain is formed by the surface of a sphere with its center at $\xi = x/c_R = 0.7$, $\eta = y/s = 0$, $\zeta = z/s = 0$ and a radius of $5c_R$, where c_R denotes the root chord and s the local semi-span.
The grid consists of eight patched blocks, the grid lines are continuous across block boundaries while the slope of the grid lines is nearly continuous. The grid contains a singular line which starts at the apex and runs in upstream direction to the outer boundary.

Results of computations

With the Euler method the flow around the delta wing has been simulated in the subsonic flow regime for a free-stream Mach number of 0.5 and in the transonic flow regime for a free-stream Mach number of 0.85. For both cases the influence of the grid density on the flow details is discussed for the wing at 20 deg angle of attack, i.e. cases with a strong leading-edge vortex. Furthermore for the transonic free-stream Mach number we consider the development of the flow with incidence, while for both cases the development of the near wake is investigated.
For all calculations the Euler method converged in 1500 to 2500 iterations, in which the root mean square norm of the time-like variation of the density dropped by four orders of magnitude, starting from the solution on the preceding grid level and from uniform free stream on the coarsest level.

The calculations were carried out on the NEC SX-2 supercomputer installed at NLR. Typical computing times are one CPU hour for a complete computation on the medium level, five CPU hours for a complete computation on the fine level of the grid.

Subsonic flow $M_\infty = 0.50$, $\alpha = 20$ deg

Solutions obtained on both levels of the grid are discussed. The result on the medium level was computed with the parameters controlling the dissipative terms at their standard setting for subsonic flow, i.e. with just the 4th-difference term switched on. It turned out that the resulting solution features a (weak) cross-flow shock. Therefore the calculations on the fine level of the grid were run with the second-order dissipative term switched on at locations with steep gradients.
The isobar pattern on the upper wing surface obtained from the computed results on the medium and fine level of the grid are shown in Fig. 3a and 3b, respectively.

For both levels of the grid the low-pressure region on the wing upper surface, forming the footprint of the leading-edge vortex, indicates that flow separation from the sharp leading-edge starts very close to the apex. The lowest values of the surface pressure coefficient are found near the apex underneath the vortex, typical for subsonic flow cases where there is a relatively large effect of the singularity at the apex as well as a relatively strong upstream influence of the trailing edge. For higher free-stream Mach numbers the region with lowest pressures moves to a more aft position on the wing, as will be shown later on.

Comparison of figures 3a and b shows that the Euler solution on the medium level of the grid and the one on the fine level of the grid do not differ in character. However, on the fine level of the grid the pressures in the suction peak are substantially lower than those found in the result on the medium level of the grid.
For both grid levels the flow on the upper wing surface is supersonic in the low-pressure region, reaching Mach numbers above 1.5 on the fine grid.

In Fig. 4a the spanwise pressure distributions as computed on the medium and the fine level of the grid are compared with each other and with experimental data (Ref. 13) for the stations x/c_R = 0.3, 0.6 and 0.8.

Comparison of the solution on the fine mesh with the one on the medium level shows that when the grid is refined, the upper-wing surface pressure peak becomes steeper and higher while its position shifts slightly in outboard direction. For all three chordwise stations considered there is an excellent agreement in the spanwise pressure distributions on the lower wing surface, as well as on the upper wing surface in the region close to the plane of symmetry and the region near the leading edge. A cross-flow shock, defined as a shock outboard of the suction peak at approximately constant percentage local semi span, is difficult to detect in these plots although upstream of x/c_R = 0.75 in the isobar patterns isobars tend to cluster (Fig. 3) and the spanwise pressure distributions steepen up in the first two sections shown in Fig. 4a.

Comparison with experimental data shows that for the lower wing surface the agreement is satisfactory for the stations x/c_R = 0.6 and 0.8. For stations upstream of x/c_R = 0.45 (not shown here) the agreement is not as good due to the presence of the body of the windtunnel model not represented in the present numerical simulation. The comparison further shows that the Euler method grossly over-predicts the suction peak on upper wing surface, also resulting in overprediction of the lift coefficient by about 15 percent. This is primarily due to the circumstance that the Euler method lacks the ability to simulate flow separation from a smooth surface, here the so-called secondary separation, without explicitly incorporating some kind of a model for such viscosity dominated phenomenon. Studies within the framework of potential-flow theory with free, rolling up, vortex sheets (Ref. 18) have indicated that inclusion of a model for smooth-body separation will lower the upper wing surface suction peak and will shift it in inboard direction, while also the spanwise pressure distribution features the plateau region just outboard of the position of secondary separation.

In Fig. 4b the spanwise distribution of the total pressure losses at the chordwise stations x/c_R = 0.3, 0.6 and 0.8 are shown. For inviscid flows without shocks the total pressure should be constant, equal to its free-stream value. In Euler methods errors are caused by the artificial dissipation introduced by the numerics. Primarily due to a fine grid resolution in the direction normal to the wing, the error in total pressure on the major part of the upper wing surface is small (less than 1% gain) for the solution obtained on both levels of the grid, with the fine level having the smallest error. The error on the lower wing surface is due to the smaller gradients in the solution an order of magnitude smaller.

Near the leading-edge there are larger errors in total pressure on both levels. In the solution obtained on the medium as well as in the solution on the fine level of the grid one observes that on the upper surface, at between 70% and 80% local span, there is a sudden increase in total pressure loss. This increase suggests the occurrence of a weak cross-flow shock just outboard of the suction peak induced by the leading-edge vortex. The reduction in total pressure and therefore presumably the strength of the shock is largest on the fine grid level and for both levels the largest on the forward part of the wing, i.e. there where the suction peak is also highest (up to -4.2 on the fine level of the grid).
Right at the leading edge, where the flow separates, without explicitly prescribing separation, a spike in the total pressure occurs.

In Fig. 5a the isobar patterns in the plane x/c_R = 0.6 obtained from the solution on the medium and the one on the fine level of the grid are presented. Fig. 5b shows the corresponding contours of equal total pressure in the same plane. These results clearly reveal the presence of a leading-edge vortex above the wing upper surface. The minimum value of the pressure, attained at the center of the vortex core, is lower for the solution on the fine level of the grid than for the solution on the medium level of the grid. The position of the center of the vortex core, taken as the position of minimum static pressure or position of maximum total-pressure loss, is almost the same for the two grids.
In the cross-flow plane isobar pattern the weak cross-flow shock is most clearly seen as a clustering of isobars in the fine grid results.

The value of total pressure loss at the center of the vortex core is higher in the fine grid solution than in the medium grid solution.
However, on the fine grid the area in which there are total pressure losses is smaller, i.e. more confined around the center of the vortex core.
Apparently for the present subsonic case the reductions due to grid refinement of the errors in total pressure cause the area in which they occur to be reduced but at the center of the core the reduction due to grid refinement cannot balance the increase of the errors associated with the resolution of steeper gradients.
Spanwise cross-sections taken all along the centerline of the wing indicate that there is very little variation with streamwise distance of the total pressure loss at the center of the vortex core.

It may be concluded that the computational results on the two levels of the grid are qualitatively the same, i.e. both solutions feature the same flow phenomena. Quantitatively there are some differences which can be understood in terms of differences in grid density, however, which are considerably smaller than the differences with experimental data.

Transonic flow M_∞ = 0.85, α = 20 deg

For this case of compressible vortex flow solutions are discissed obtained on the medium and fine level of the grid. The solutions on both levels were obtained with the parameters controlling the dissipative terms set at their standard values for transonic flow, i.e. with the fourth-difference term switched on, the second-difference term taking over at locations with sharp gradients.

In figure 6a the upper wing surface isobar pattern for 20 deg incidence is presented for the medium

level, in figure 6b for the fine level of the grid. Both figures indicate that the formation of the vortex starts very close to the apex. Furthermore, in both pictures the closely-spaced isobars outboard of the pressure minimum indicate the presence of a "cross-flow shock", most clearly so on the rear part of the wing. On this part of the wing also a second shock appears which, at about 93% root chord merges with the cross-flow shock, forming a Y-shaped shock system, with as stem the strong cross-flow shock downstream of the 93% root chord station. On the central part of the wing at about 83% root chord a third shock appears, the so-called "rear shock". This weak shock is normal to the plane of symmetry and extends some distance in the direction of the leading-edge. Comparison of the upper wing surface isobar pattern of the solution on the fine with the one of the solution on the medium mesh shows that the shocks are steeper, but more importantly, that no new flow features evolve.

Compared to the pressure distribution at the lower Mach number the suction peaks are much reduced and in height about constant in chord-wise direction, i.e. at least on the forward part of the wing the solution is more conical in appearance.

In figure 7a (note change in vertical scale compared with Fig. 4a) the spanwise pressure distributions computed on the fine and the medium grid are compared with each other and with experimental data of the International Vortex Flow Experiment (Ref. 12). Results are shown at the same three spanwise stations that we considered at the lower Mach number. In addition to these spanwise sections figure 8 presents the pressure distribution along the chordwise section situated in the plane of symmetry. In the computed results (Fig. 7a) the cross-flow shock is located between 70 and 75% local semi-span, in the measured data the much weaker cross-flow shock is situated further inboard, namely at about 60% local semi-span. The experimental data further indicate, as may be concluded from the pronounced second suction peak, that the cross-flow shock provokes an early secondary separation that results in a relatively strong secondary vortex. As for the case of subsonic vortex flow it is clear that in order to improve the correlation of the numerical simulation with experiments secondary separation effects must be included in the simulation. However, because of the less negative pressures for the higher Mach number for the present case the effect of secondary separation is less severely felt in the integrated forces and moments.

At x/c_R = 0.8 the level of the pressure on the upper wing surface near the plane of symmetry is much lower than measured. Fig. 8 shows that this can be attributed to the difference in the measured and the predicted position of the "rear shock". Fig. 8 also proves that on the fine level of the grid the "rear shock" is better resolved, but still at the same position as on the medium level of the grid.
It may be expected that the position and strength of the leading edge vortex, the cross-flow shock and the rear shock are strongly interrelated. Improving the simulation by including a secondary separation model will affect all three flow features.

For the lower wing surface the agreement of computed and measured pressure distributions is excellent, except near the apex where the influence of the body is greatest.
In terms of lift coefficient the Euler solutions result in values which are about 7.5% higher than the value found in the experimental investigation.

Comparison of the results on the medium and on the fine level of the grid indicates that for the surface pressure distribution increasing the grid density
-results in a steeper but also somewhat stronger "cross-flow shock"
-shifts the suction peak, i.e. the position of the vortex, slightly inboard
-steepens the "rear shock"
-has no effect on the lower wing surface pressure distribution.

In figure 7b (note change in vertical scale compared to Fig. 4b) spanwise sections of the distribution of the total pressure are presented for x/c_R = 0.3, 0.6 and 0.8. It shows that as the flow passes through the cross-flow shock the total pressure is reduced by 13-14% on the medium level and by 23-24% of its free-stream value on the fine level of the grid. For the latter grid the shock is stronger, which explains the larger loss in total pressure. As expected it is indicated that away from the shock the errors in total pressure are smaller on the fine level of the grid than those on the medium level of the grid and comparable to those encountered at the lower Mach number.

Fig. 9 presents the isobar pattern in the plane x/c_R = 0.6 and the corresponding pattern of contours of equal total pressure in the same plane obtained from the solution on the fine level of the grid. Corresponding plots for the medium level of the grid are included in Figs. 12a and b (bottom sub-figure).
For this case of compressible vortex flow the cross-flow shock is strong and clearly shows up in both the patterns of contours of equal static and those of equal total-pressure. The shock appears to bridge the gap between the wing upper surface and the vortical flow region. Outboard (i.e. downstream) of the cross-flow shock and underneath the shear layer emanating from the leading edge there exists a relative large region where both the static and total pressure are only slowly changing. Especially on the fine level of the grid (Fig. 9), where the shock is somewhat stronger, this is a rather extensive portion of the flow field.
The "rear shock" is clearly visible in the isobar pattern in the plane of symmetry (Fig. 10), obtained from the solution on the fine level of the grid. Although it is a weak (normal) shock it extends quite some distance into the flow field.

The cross-flow-plane contours of the equal total pressure show that at the center of the vortex core the total pressure drops to 45 percent of its free stream value, both on the medium and on the fine level of the grid, i.e. giving at the center of the vortex core about 20% more total pressure loss than we found for subsonic flow. Further note that compressibility has a considerable effect on the shape of the vortex core. Increasing the Mach number results in a more flattened vortex core which as a result of the interaction with the

cross-flow shock is at a more inboard location. As for the lower Mach number the total pressure loss at the center of the core does not vary very much with longitudinal distance along the vortex core.

Comparing the cross-flow-plane results obtained on the medium level of the grid (Fig. 12a and b, lower figures) with those obtained on the fine level (Fig. 9) one observes in addition to the points already noted in the discussion of the surface quantities that on the fine level of the grid the region of the flow field with total pressure losses has shrunk in dimension. However, the minimum total pressure, which occurs at the center of the vortex core, is about the same for both levels of the grid. It is hypothesized that as far as the total-pressure loss near the center of the core is concerned here also refining the mesh tends to decrease the discretization error and at the same time increases the gradients in the flow solution and thus the discretization error, now apparently such that, on this grid for this free stream flow condition and this setting of the artificial dissipation parameters, the net effect is about the same loss in total pressure.

The first overall conclusion that can be drawn for this flow condition is very similar to the one drawn for the subsonic flow condition at the end of the preceding section, namely that grid refinement does not resolve in new flow features and differences between computed and measured results, considerably smaller here, are due to the Euler method not simulating secondary separation. The second conclusion is that effects due to compressibility result in very significant changes in the flow solution, not unlike those found in the experimental investigation of for instance Ref. 19 for a similar configuration.

Variation of the solution with incidence, $M_\infty = 0.85$

This section considers for the transonic flow case the development of the flow with angle of attack, i.e. numerical results are presented for α = 10, 15 and 20 deg. Since the preceding sections indicate that the grid density of the medium level of the grid suffices to resolve most details of the flow only results on this level of the mesh have been computed for the lower incidences.

Figure 11a shows the development of the spanwise pressure distribution with increasing incidence at $x/c_R = 0.6$, which is typical for the distribution on the forward and central portion of the wing. The figure indicates that as the angle of attack is increased and the vortex increases in strength, the suction peak on the upper wing surface grows in height and in width and moves in inboard direction while on its outboard (i.e. downstream) flank the "cross-flow shock" develops.
The re-attachment point on the upper wing surface (the point of locally maximum pressure), which at 10 deg is at 60% local semi span has at 20 deg moved to the plane of symmetry. On the lower wing surface the pressure increases gradually, while the (primary) attachment point moves away from the leading edge, i.e. from a point at 95 to a point at 80% local semi-span location. Increasing the incidence slightly further will move the primary attachment point to the plane of symmetry also.

Figure 11b presents the development with incidence of the chordwise pressure distribution along the intersection of the wing with the plane of symmetry. It clearly shows the development of the "rear shock" on the upper surface at 15 and 20 deg incidence. At α = 10 deg the flow in the plane of symmetry is still sub-critical.
At the apex there is a distinct (suction) spike in the pressure distribution, indicative for a singularity at that point.

Figures 12a and b illustrate for $x/c_R = 0.6$ the development with incidence of the flow field about the forward and central part of the wing. These figures show the gradual, nearly conformal, development of the region with significant total pressure losses (i.e. the region with vortical flow). The center of the vortex core moves inboard and upward. Furthermore the region on the upper surface influenced by the vortex becomes larger.
It further shows how, in the flow field above the upper surface, the cross-flow shock developes accompanied by a gradually more backward leaning of the isobars around the center of the vortex core. With increasing incidence the static pressure and the total pressure at the center of the core decrease, indicative for a stronger vortex with steeper gradients near its center.

Flow field near the trailing edge

In this section the development of the flow just upstream of the trailing edge and in the near wake just downstream of the trailing edge is considered in some detail for the wing at 20 deg incidence and for both the subsonic and the transonic free-stream Mach number. This region of the flow field is of extreme importance for cases at somewhat higher incidences where the experiments (Refs. 12, 13) have shown that vortex breakdown occurs. The objective of the present study is to investigate how the wake just downstream of the trailing edge, i.e. the near wake, develops. For subsonic flow it has been shown (Ref. 20) that downstream of the trailing edge a complex vortex wake develops. The constitutive elements of this mushroom-shaped vortex wake are the leading-edge vortex and the so-called trailing-edge vortex. The latter vortex contains vorticity of sign opposite to that contained in the leading-edge vortex and forms immediately downstream of the trailing edge. Although the sign of the vorticity in the trailing-edge vortex is the same as that in the secondary vortex resulting from the secondary separation it is a different vortex. It forms, even in inviscid flow, as a consequence of the wake in the plane x/c_R = 1.0 containing vorticity of both signs, i.e. negative in the shear layer between the plane of symmetry and the wing tip, positive in the shear layer from the leading edge and in the leading-edge vortex (Ref. 18).

Figure 13a shows for $M_\infty = 0.50$, α = 20 deg the contours of equal total pressure in five consecutive planes x/c_R = constant, namely x/c_R = 0.95, 1.0, 1.025, 1.0 and 1.10, as obtained from the solution on the fine level of the grid. This figure indeed indicates the formation of a wake with two regions of increased total pressure losses, indicative for regions with vortical flow.
In the near wake the leading-edge vortex can be identified as the continuation of the structure depicted in Fig. 5b in the plane $x/c_R = 0.8$ and in the top two plots of Fig. 13a. This vortex moves outboard and upward. Apparently because in the region considered the grid is still relatively fine

and not yet stretching too much the vortex remains compact and is not diffused. The level of the total pressure losses at the center of the core stays the same (~ 35-40%).
The formation of the trailing-edge vortex starts right at the trailing edge (x/c_R = 1.0) as evidenced by the local maximum (0.15) in the total pressure loss at about 90% semi-span, caused by the high gradients in the solution in that region. Further downstream a vortex-like structure develops with increasing total pressure losses at its center. Indeed a mushroom-shaped vortex wake, consisting of the leading-edge and the trailing-edge vortex evolves.

For the transonic case (M_∞ = 0.85, α = 20 deg) the contours of equal total pressure are presented in Fig. 13b, for the same 5 cross-flow planes, again obtained from the solution on the fine grid. For the case of compressible vortex flow the situation is complicated by the presence of the strong cross-flow shock. It follows from figure 13b that downstream of the trailing edge the cross-flow shock has disappeared (between x/c_R = 1.01 and 1.025). As for the lower Mach number the leading-edge vortex continues downstream of the trailing edge, again without much diffusion, but now it does not appear to move upward and outboard that much. Furthermore, the formation of the trailing-edge vortex, by the roll-up of the wake, is now more vigorously resulting in higher total pressure losses at its center. At x/c_R = 1.1 the wake has again a mushroom-shaped structure but now occupying a larger area in the cross-flow plane than is the case for the lower Mach number.
In the first three cutting planes presented in Fig. 13b an additional flow feature is identified, characterised by a local minimum in the total pressure distribution. This feature can be traced back to the kink in the leading edge, i.e. to x/c_R = 0.85, and is termed the "tip vortex". Seen in consecutive cross-flow planes this vortex travels around the leading-edge vortex and at x/c_R = 1.05 is so close to the core of the leading-edge vortex that it can no longer be distinguished and may be assumed to be fully merged with the latter.

Concluding remarks

Results of an Euler method have been obtained for subsonic (M_∞ = 0.50) and transonic (M_∞ = 0.85) vortex flow around a 65-deg cropped delta wing. The calculations were carried out on the medium (~ 150K cells) and fine level (~ 1.2M cells) of a high-quality grid.
It is demonstrated that the results on the two levels of the grid are qualitatively the same. The solution on the fine level of the grid does not reveal any flow features not already present in the solution on the medium level of the grid. However, in regions with large gradients the resolution of flow details is improved on the fine grid level.

The differences between the computed surface pressure distributions mutually are smaller than those between computed pressure distributions and experimental data. The differences between theory and experiment are primarily due to the effect of secondary separation, which is not modeled in the present numerical simulation. To obtain a better agreement between theory and experiment it is necessary to include some modeling of the effect of secondary separation in the simulation.

For the 65-deg swept cropped delta wing there is a substantial effect of compressibility on the flow solution. At transonic speed a strong "cross-flow shock" develops on the forward part of the wing, a "Y-shaped" cross-flow shock and a "rear shock" on the aft part of the wing. It is shown that these shocks develop quite gradually for the incidence increasing from 10 to 20 deg (still below the onset of vortex breakdown).
It is demonstrated that the Euler method is capable of simulating in the near wake of the wing the mushroom-shaped vortex structure formed by leading-edge and trailing-edge vortex. This investigation has also revealed the occurrence, at transonic speed, of a third vortex, termed the "tip vortex".

References

1. Hoeijmakers, H.W.M., Methods for Numerical Simulation of Leading-Edge Vortex Flow, In Studies of Vortex Dominated Flows, ed. M.Y. Hussaini and M.D. Salas, Springer Verlag, pp. 223-269, 1987. Also NLR MP 85052 U.
2. Murman, E.M., Rizzi, A.; Applications of Euler Equations to Sharp-Edge Delta Wings with Leading Edge Vortices, AGARD CP412, Paper 15 (1986).
3. Longo, J.M.A., The Role of the Numerical Dissipation on the Computational Euler-Equations-Solutions for Vortical Flows, AIAA Paper 89-2232 (1989).
4. Hitzel, S.M., Wing Vortex-Flows up into Vortex Breakdown. A Numerical Simulation, AIAA Paper 88-2518 (1988).
5. O'Neil, P.J., Barnett, R.M., Louie, C.M., Numerical Simulation of Leading-Edge Vortex Breakdown Using an Euler Code, AIAA Paper 89-2189 (1989).
6. Raj, P., Sikora, J.S., Keen, J.M., Free-Vortex Flow Simulation using a Three-Dimensional Euler Aerodynamic Method, J. of Aircraft, Vol. 25, No. 2 (1988).
7. Wardlaw Jr., A.B., Davies, S.F., Euler Solutions for Delta Wings, AIAA Paper 89-3398 (1989).
8. Fujii, K., Obayashi, S., High-Resolution Upwind Scheme for Vortical Flow Computations, J. of Aircraft, Vol. 26, No. 12, pp. 1123-1129 (1989).
9. Hsu, C.-H. Liu, C.H., Upwind Navier-Stokes Solutions for Leading-Edge Vortex Flows, AIAA Paper 89-0265 (1989).
10. Ghaffari, F., Luckring, J.M., Thomas, J.L., Bates, B.L., Navier-Stokes Solutions about the F/A-18 Forebody-LEX Configuration, AIAA Paper 89-0338 (1989).
11. van den Berg, J.I., Boerstoel, J.W., Development and Validation of a Characteristic Boundary Condition for a Cell-Centered Euler Method, ICAS Paper 90-6.9.3 (1990).
12. Elsenaar, A., Eriksson, G., Proceedings of the Symposium on "International Vortex Flow Experiment and Euler Code Validation", Stockholm, Oct. 1-3 (1986).
13. Elsenaar, A., Hoeijmakers, H.W.M. An Experimental Study of the Flow Over a Sharp-Edged Delta Wing at Subsonic, Transonic and Supersonic Speeds, Paper presented at AGARD FDP Symposium Vortex Flow Aerodynamics, Oct. 1990.

14. Jacobs, J.M.J.W., Hoeijmakers, H.W.M., Aspects of the Application of an Euler-Equation Method to the Simulation of Leading-Edge Vortex Flow, In Proceedings of 8th GAMM Conference on Numerical Methods in Fluid Mechanics, September 1989, Delft, The Netherlands. Also NLR MP 89272 U (1989).
15. Jacobs, J.M.J.W., Kassies, A. Boerstoel, J.W., Buijsen, F., Numerical Interactive Grid Generation for 3D Flow Calculations, In: Numerical Grid Generation in Computational Fluid Mechanics '88, Pineridge Press, (1988) pp. 925-943.
16. Boerstoel, J.W., Progress Report of the Development of a System for the Numerical Simulation of Euler Flows, with Results of Preliminary 3D Propeller-Slipstream/Exhaust-Jet Calculations, NLR TR 88008 U (1988).
17. Jameson, A, Schmidt, W., Turkel, E., Numerical Solution of Euler Equations by Finite Volume Methods Using Runge-Kutta Time-Stepping Scheme, AIAA Paper 81-1259 (1981).
18. Hoeijmakers, H.W.M., Computational Aerodynamics of Ordered Vortex Flows, NLR TR 88088 (1989).
19. Bannink, W.J., Houtman, E.M., Ottochian, S.P., Investigation of the Vortex Flow over a Sharp-edged Delta Wing in the Transonic Speed Regime, Report LR-594, Faculty of Aerospace Engineering, Delft University of Technology (1989).
20. Hummel, D., On the Vortex Formation over a Slender Wing at Large Angles of Incidence, AGARD CP247, Paper 15, (1979).

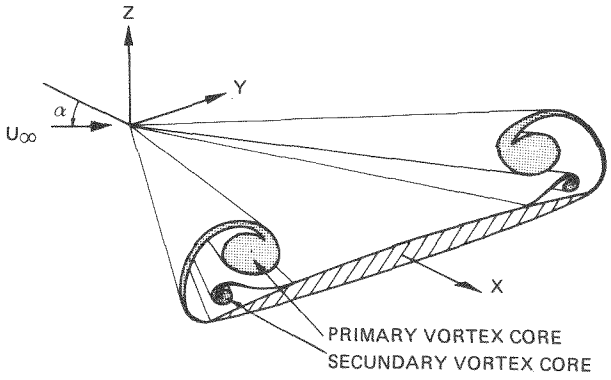

Fig. 1. Vortex flow about a delta wing

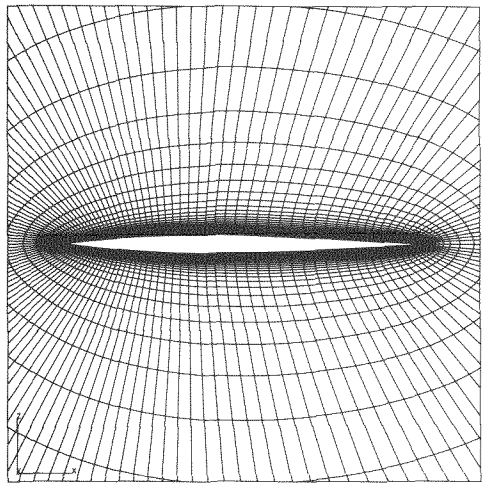

a) Plane of symmetry

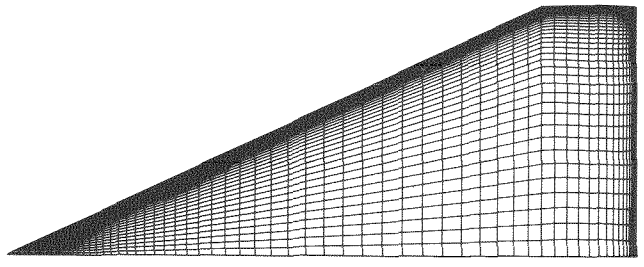

b) Wing upper surface (72 x 38)

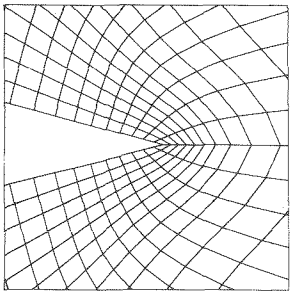

$x/c_R = 0.5$

c) Leading edge

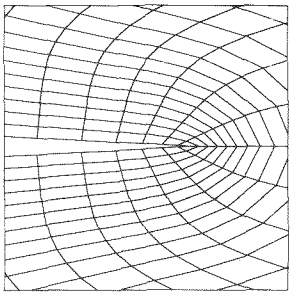

$y/s = 0.5$

d) Trailing edge

Fig. 2. Details of medium level of grid used in present investigation

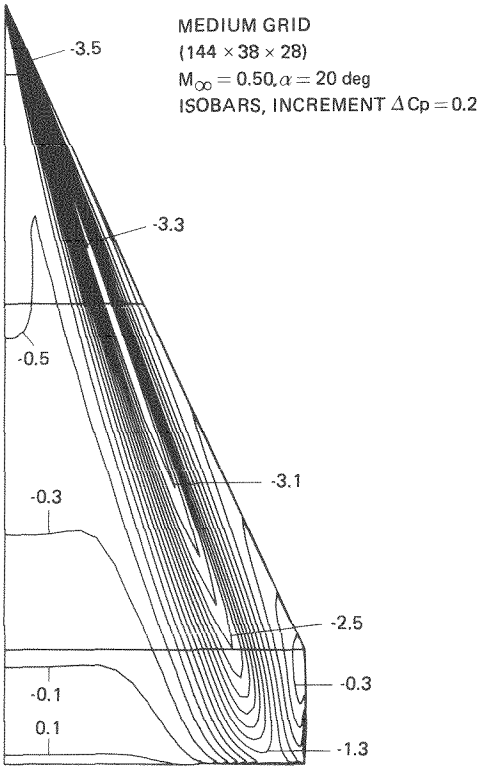

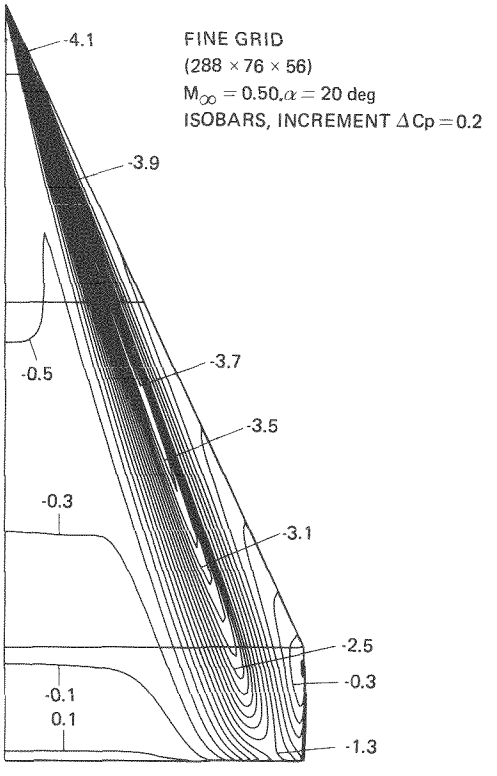

Fig. 3. Isobars on wing upper surface, different grid densities, subsonic flow

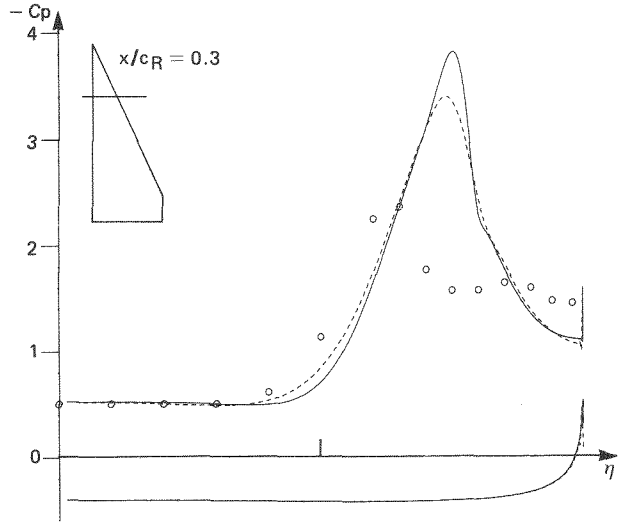

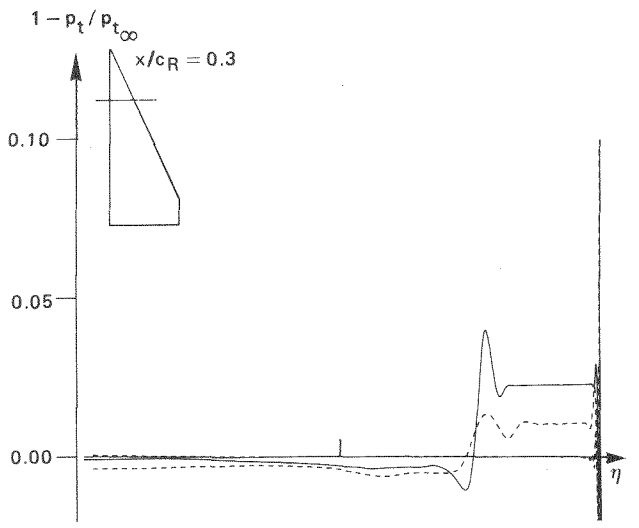

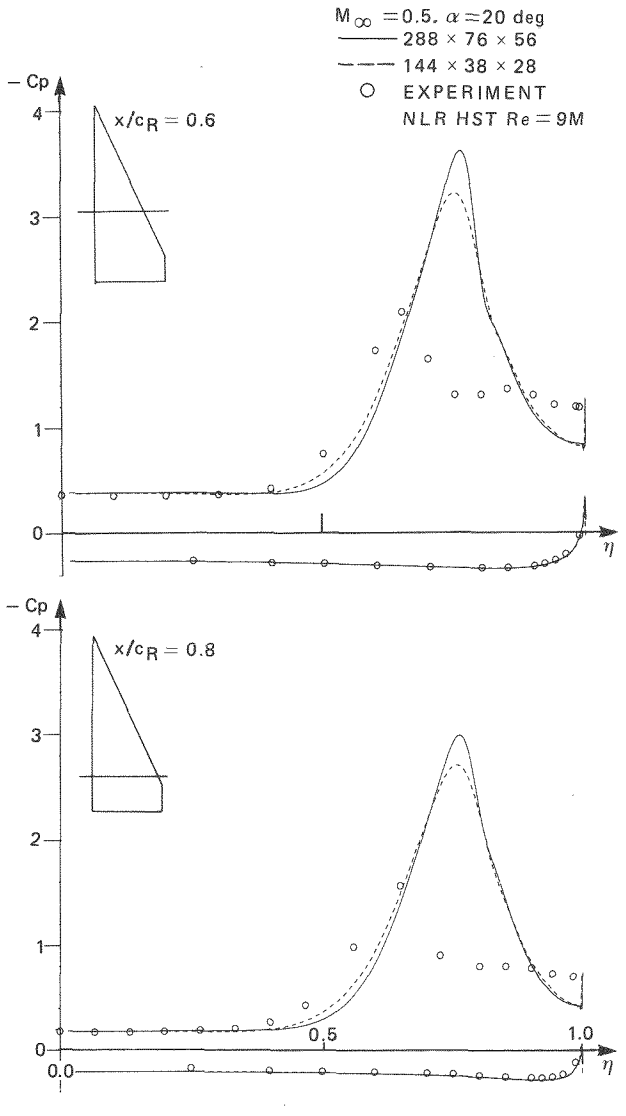

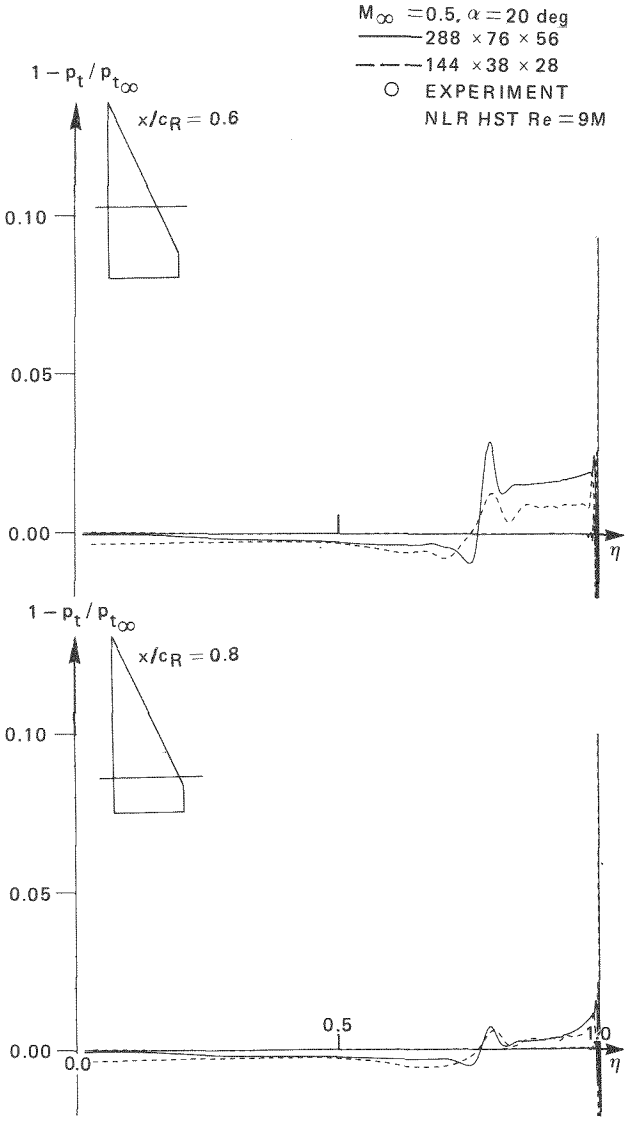

Fig. 4. Spanwise pressure distribution, different grid densities, subsonic flow

Fig. 4b. Spanwise distribution of total pressure, different grid densities, subsonic flow

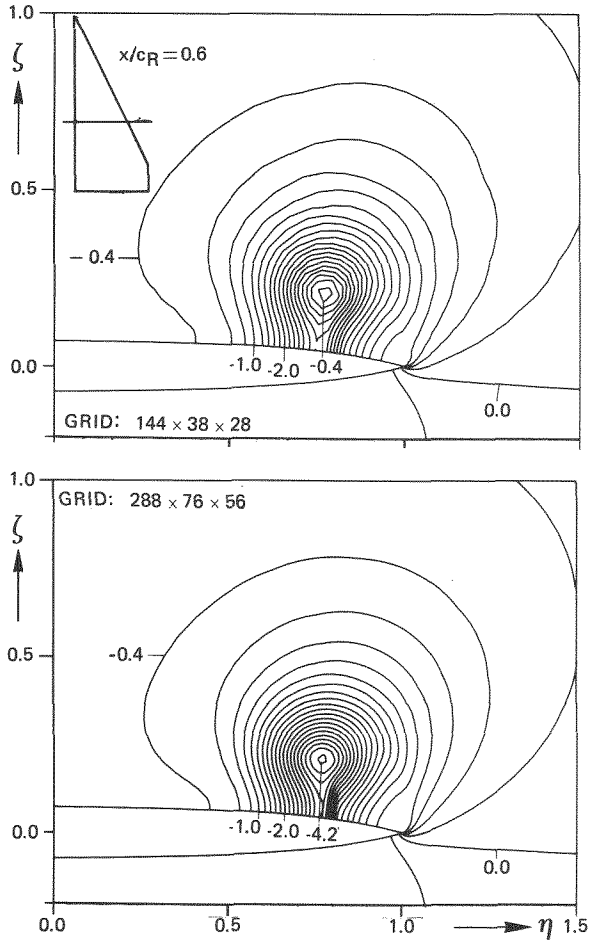

INCREMENT: $\Delta Cp = 0.2$

$M_\infty = 0.5, \alpha = 20$ deg

Fig. 5a. Isobars in plane x/c_R = 0.6, different grid densities, subsonic flow

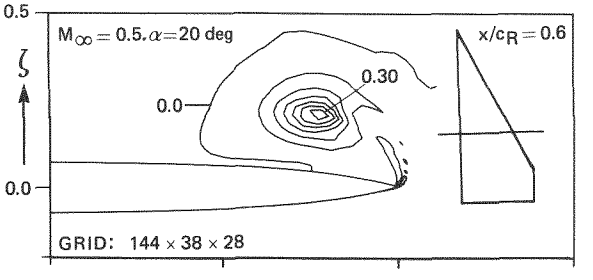

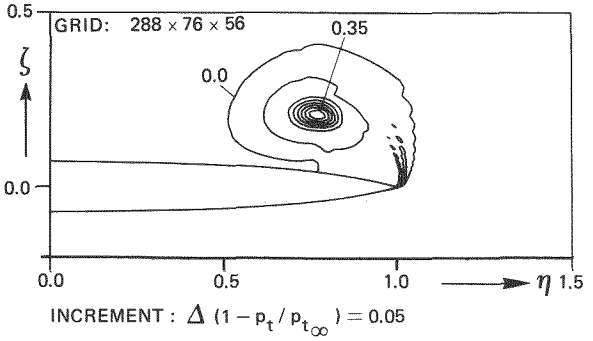

INCREMENT: $\Delta (1 - p_t / p_{t_\infty}) = 0.05$

Fig. 5b. Contours of equal total pressure in plane x/c_R = 0.6, different grid densities, subsonic flow

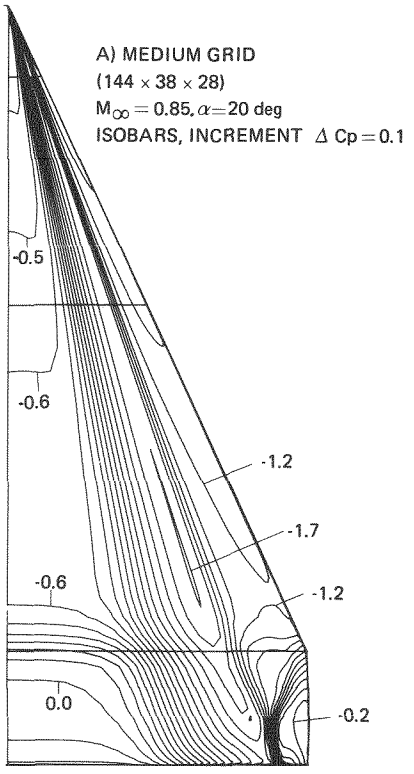

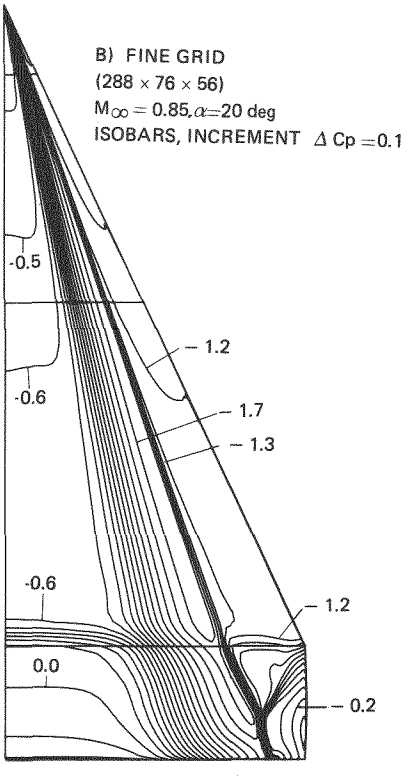

Fig. 6. Isobars on wing upper surface, different grid densities, transonic flow

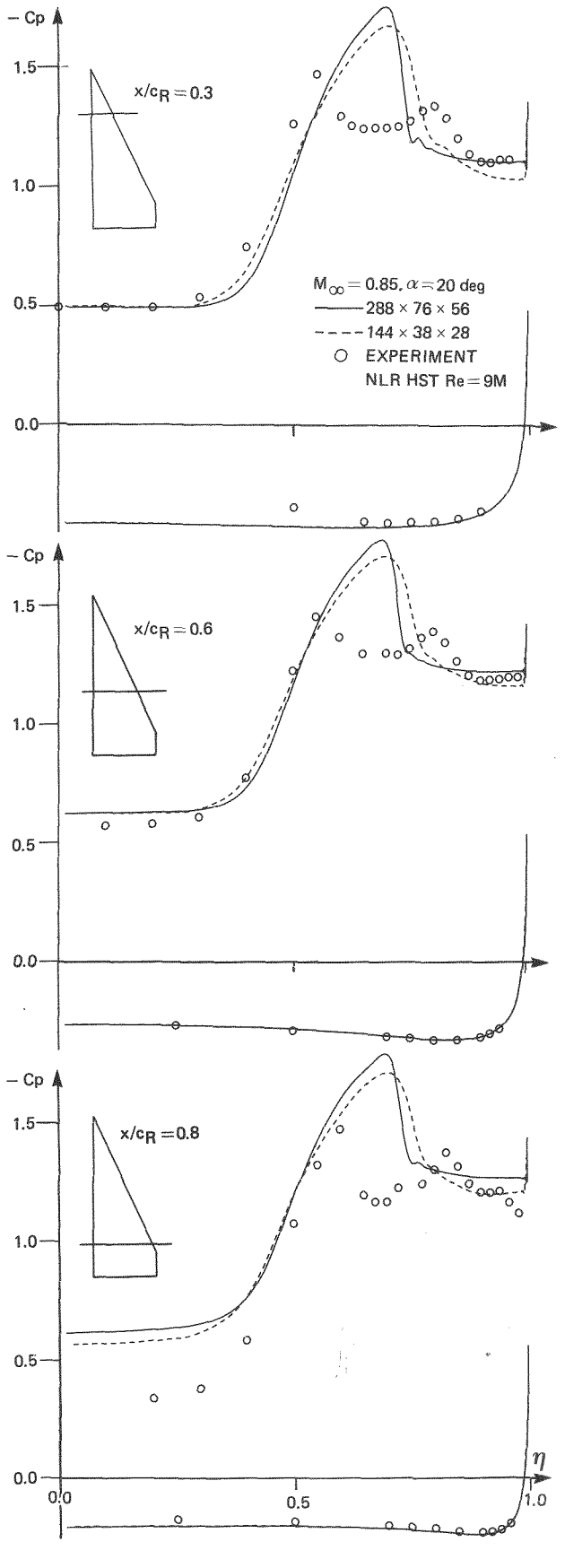

Fig. 7a. Spanwise pressure distribution, different grid densities, transonic flow

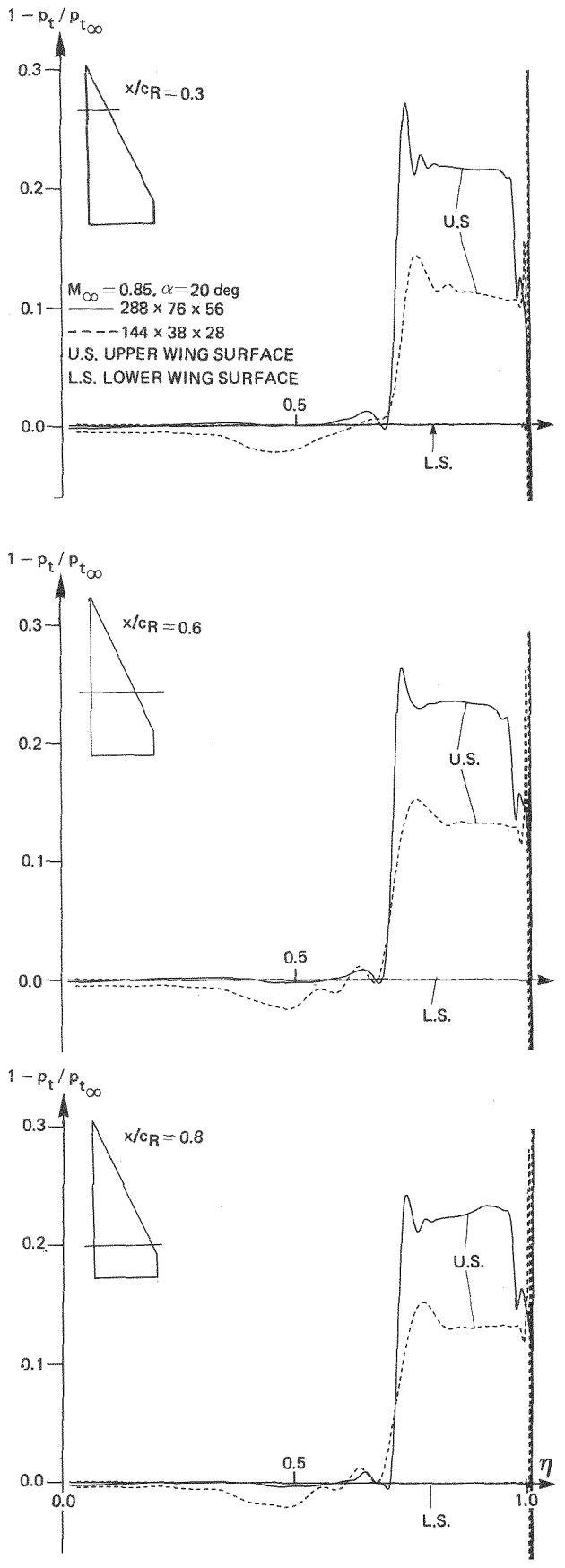

Fig. 7b. Spanwise distribution of total pressure, different grid densities, transonic flow

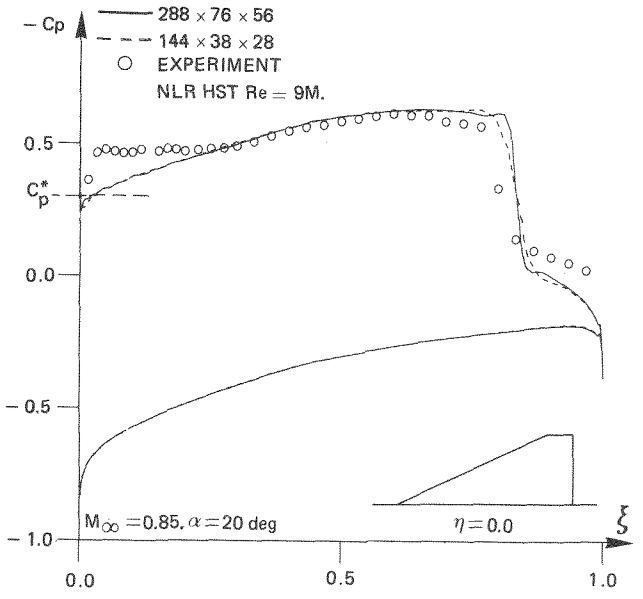

Fig. 8. Chordwise pressure distribution, different grid densities, transonic flow

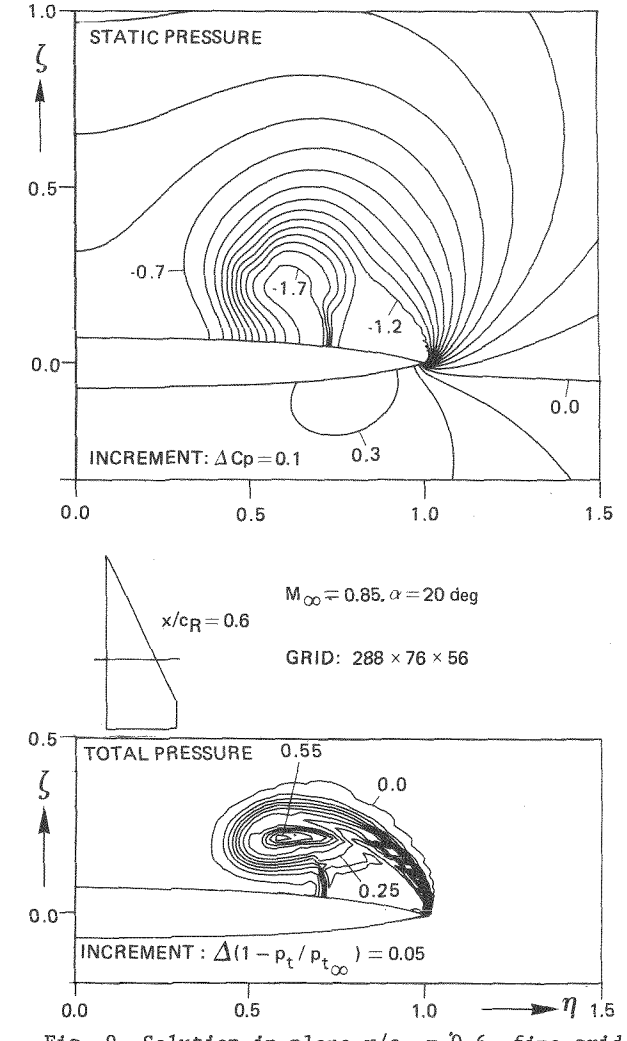

Fig. 9. Solution in plane $x/c_R = 0.6$, fine grid level, transonic flow

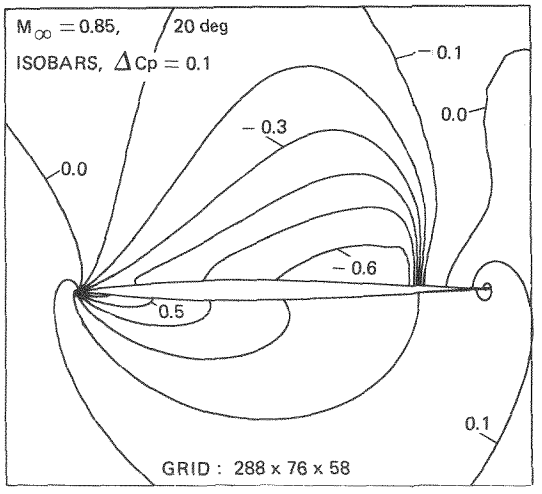

Fig. 10. Isobars in plane y/s = 0.0, fine grid level, transonic flow

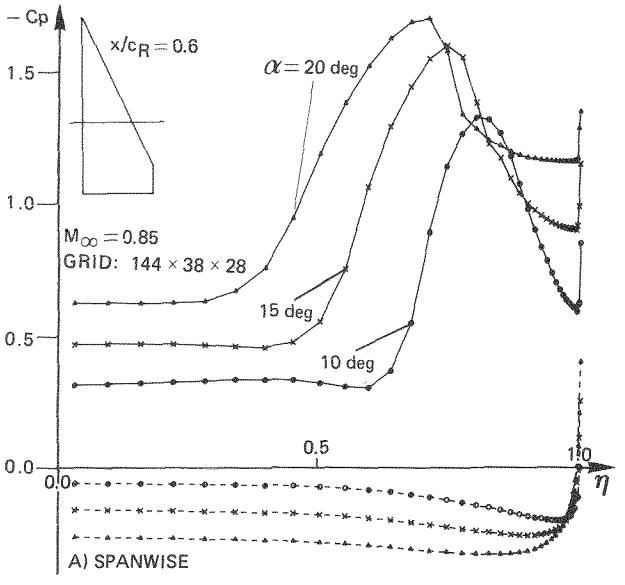

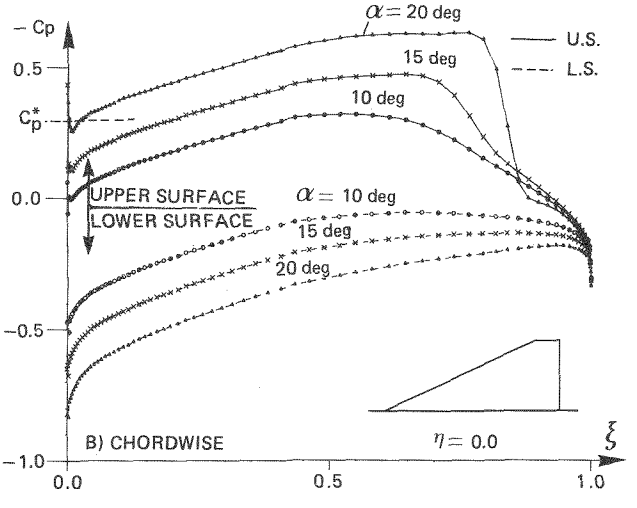

Fig. 11. Development of surface pressure distribution with incidence, transonic flow

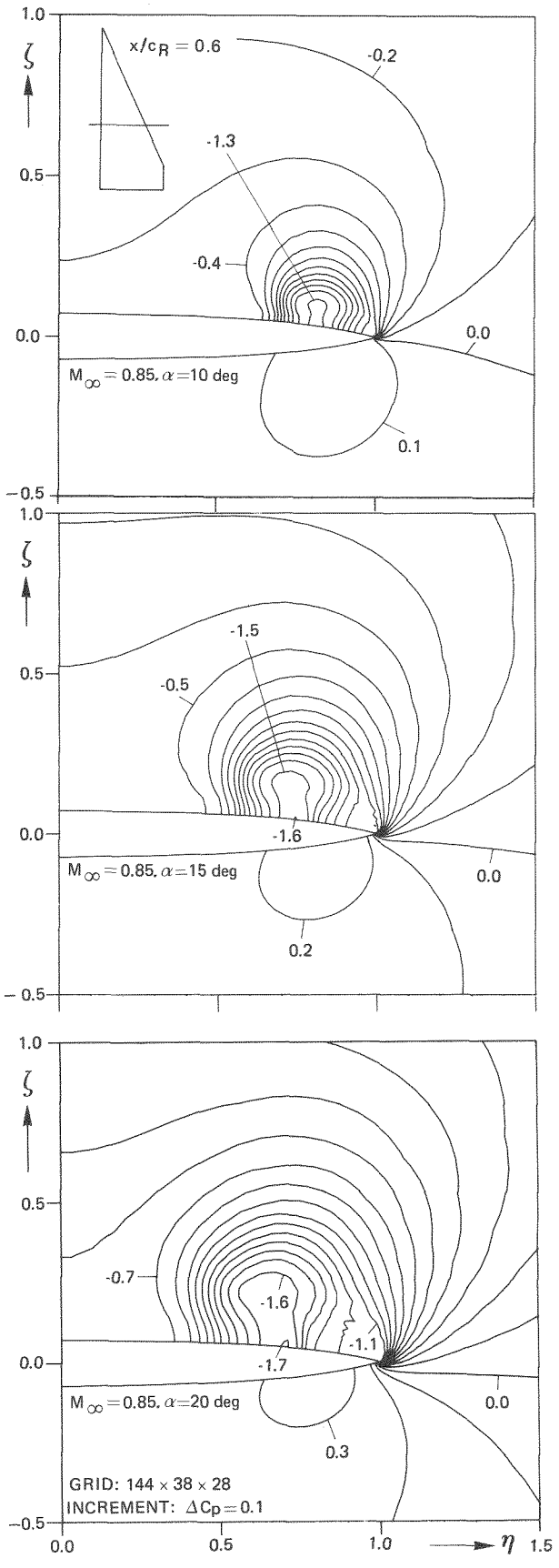

Fig. 12a. Isobars in plane $x/c_R = 0.6$, medium grid level, transonic flow, different incidences

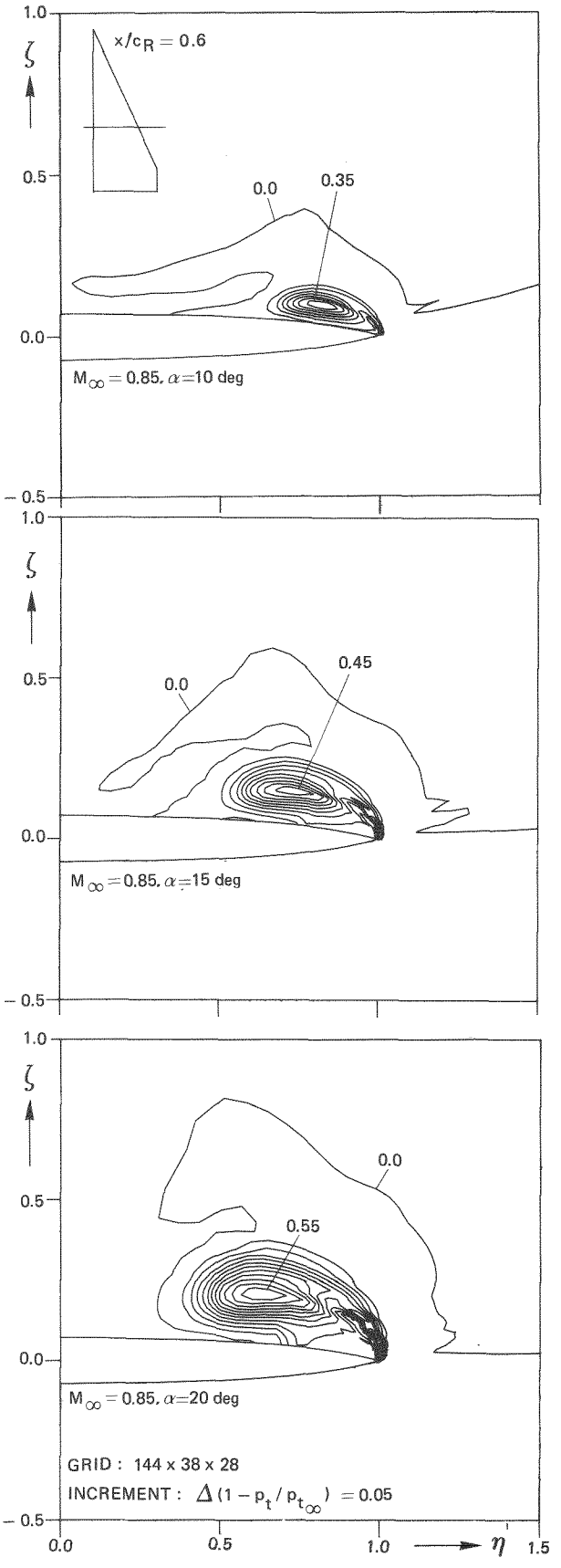

Fig. 12b. Contours of equal total pressure in plane $x/c_R = 0.6$, medium grid level, transonic flow, different incidences

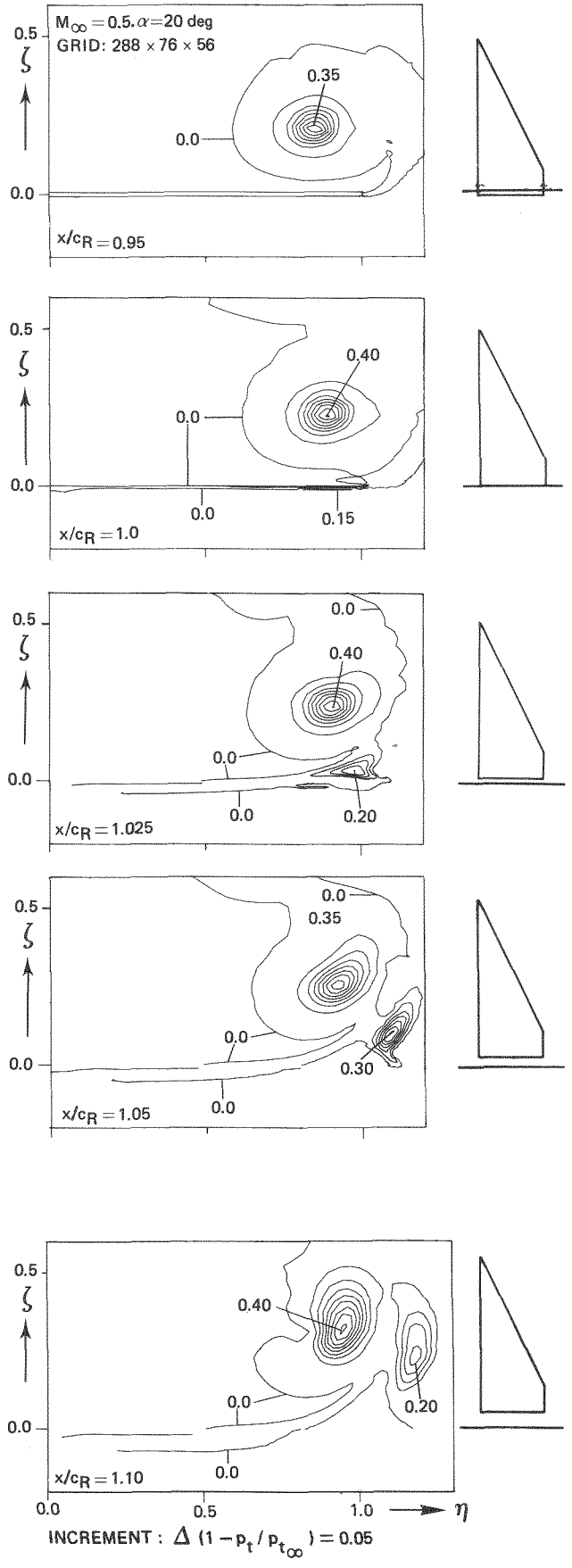

Fig. 13a. Contours of equal total pressure in planes x/c_R = constant, fine grid level, subsonic flow

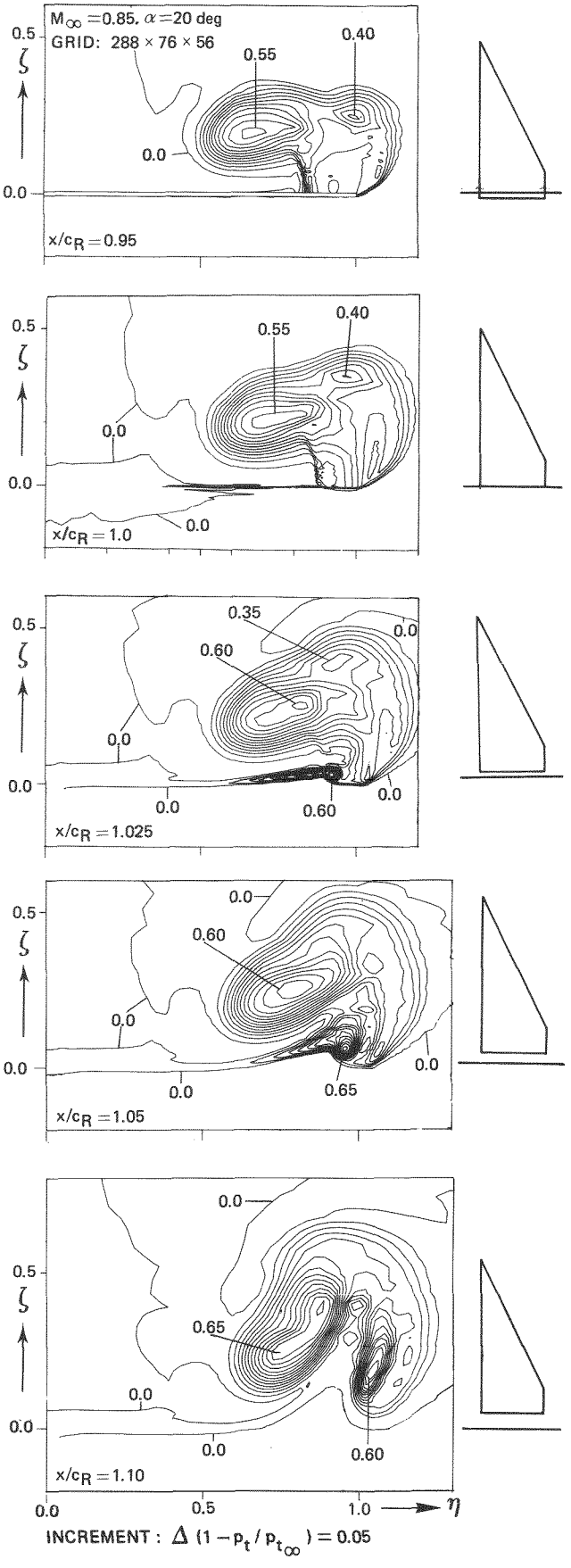

Fig. 13b. Contours of equal total pressure in planes x/c_R = constant, fine grid level, transonic flow